Journal of Sound and Vibration (2001) **243**(5), 823–846
doi:10.1006/jsvi.2000.3479, available online at http://www.idealibrary.com on IDEAL®

MECHANISMS FOR SOUND GENERATION IN INVISCID TWO-DIMENSIONAL VORTEX INTERACTIONS

S. K. TANG

Department of Building Services Engineering, The Hong Kong Polytechnic University, Hong Hom, Kowloon, Hong Kong, People's Republic of China. E-mail: besktang@polyu.edu.hk

AND

N. W. M. KO

Department of Mechanical Engineering, The University of Hong Kong, Hong Kong, People's Republic of China

(*Received* 4 *April* 2000, *and in final form* 29 *August* 2000)

Theoretical and numerical results obtained in the present investigation illustrate that the motions of the vorticity centroids and the unsteady deformation of the vortex cores are the sources of sound in the inviscid two-dimensional vortex interactions at low Mach number. A theory for the sound generation, based on the low Mach number vortex sound theory, is developed and the relationship between the core deformation and sound radiation for slightly deformed vortices is explicitly found. The unsteady vortex core deformation is also found to be important in all the interaction cases discussed.

1. INTRODUCTION

It is now well known that sound can be generated by turbulent flow. The fundamental aeroacoustics theory of Lighthill [1] pioneered this branch of research. Many models for turbulent sound generation have been developed in the past few decades. Typical examples include the wave antenna of Crow [2], the vortex sound theory of Powell [3], the instability wave model of Ffowcs Williams and Kempton [4] and the stagnation enthalpy of Doak [5]. However, from the stress tensor of Lighthill [1] to the more recent stagnation enthalpy of Doak [5], the theoretical sound sources are abstract and very often not physically measurable. The experimental development, therefore, seriously lags behind the theoretical one such that some of the theoretical deductions have not yet been confirmed. The question of how sound is produced by turbulent structures remains open.

The advance in computing technology allows the direct numerical simulation of sound production by a turbulent flow. Colonius *et al.* [6] and Mitchell *et al.* [7] found that the conventional acoustical analogy has given rise to source terms that may not have contribution in the overall sound field produced by a shear layer. Though their results show some essential features of the experimental sound field, the source terms they used involve local fluid velocities and their gradients, which can hardly be measured. The relationships between these terms and the turbulent structure activities are not clearly understood.

Owing to the difficulty in tackling turbulent flow, one may focus the study on a simpler flow—the vortices. The vortices, though they are drastic simplifications of the real flow, can

0022-460X/01/250823 + 24 $35.00/0

still provide insights into the physics of many practical flows. Typical studies are those of Acton [8] and Stansby and Slauoti [9]. Powell's theory of vortex sound [3] provides a framework for the study of turbulent sound using vortices. The results of Möhring [10] and Leung *et al.* [11] show that the pairing of two thin inviscid vortex rings can produce a sound field having the essential characteristics of jet noise. The results of the numerical studies of the authors [12–14], using the method of contour dynamics, have illustrated the importance of vortex acceleration and jerk in the production of sound. This observation appears to be consistent with the experimental results of Laufer and Yen [15] and Tang and Ko [16]. At least to the knowledge of the authors, Tang and Ko [16] is the first direct comparison between theory and experiment in the long quest for the sound generation due to the vortical structure dynamics in an air jet.

Two-dimensional vortical structures are commonly found in plane shear layers [17]. They undergo leapfrogging and coalescence within these shear layers and are responsible for the growth of the shear layer [17]. Though the results of Tang and Ko [14] suggest that the sound so produced is the result of the unsteady motions of the vorticity centroids of these structures, the actual sound generation mechanisms are not well understood. Differences and similarities in the sound generation mechanisms in the leapfrogging and coalescence are not explored. Thus, the present paper is an attempt to extend the above work of the authors for a deeper understanding on the sound generation mechanisms. It is hoped that the present results can provide useful information towards the development of a generalized theory for sound generation by finite core vortex interactions at low Mach number.

2. THEORETICAL CONSIDERATIONS

2.1. METHOD OF CONTOUR DYNAMICS

This method was first developed by Zabusky *et al.* [18] for the calculations of non-linear vortex patch evolution. The boundaries of the vortex cores are treated as contours. The velocity of each element on these boundaries is calculated by using the Biot–Savart induction law in the presence of vorticity. The fluid velocity, $\mathbf{u}$, at a point, $\mathbf{y}$, in the flow field is related to the local streamfunction ψ as

$$\mathbf{u} = \nabla \times (\psi \hat{y}_3), \tag{1}$$

where $\hat{y}_3$ is a unit vector in the vortex spanwise direction. The vorticity transport equation for incompressible flow suggests

$$\mathrm{D}\omega/\mathrm{D}t = 0, \tag{2}$$

where t is the interaction time and ω the vorticity at the point $\mathbf{y}$. The calculation of $\mathbf{u}$ involves an integration over the cross-sections of the vortex cores, which can be transformed into a contour integral using the Stoke's theorem. Full details on the application of this method in the two-dimensional vortex system can be found, for example, in Zabusky *et al.* [18], Dritschel [19] and some previous works of the authors [13, 14]. Thus, they are not repeated here.

2.2. VORTEX SOUND GENERATION MECHANISMS

The vortex sound theory of Powell [3] shows that the farfield pressure fluctuations, p, produced by the unsteady low Mach number motions of vorticity-bearing fluids can be

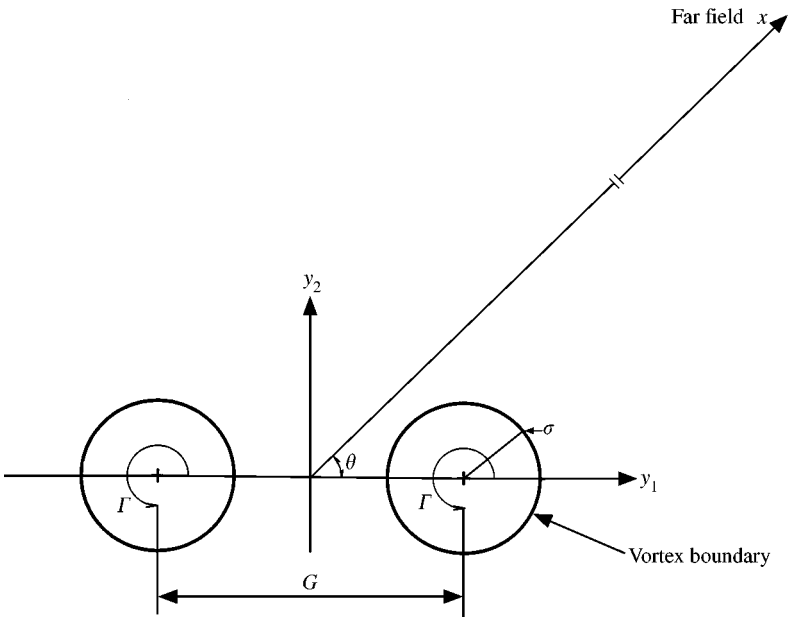

Figure 1. Schematic diagram of vortex interaction system.

obtained by solving the following inhomogeneous equation:

$$\frac{1}{c^2}\frac{\partial^2 p}{\partial \tau^2} - \nabla^2 p = \rho_0 \nabla\cdot(\omega \times \mathbf{u}), \tag{3}$$

where c and ρ_0 are the speed of sound in and the density of the ambient fluid, respectively, and τ is the observer time. The general solution of equation (3) for p at a farfield displacement $\mathbf{x}$ is, according to Möhring [10]:

$$p(\mathbf{x}, \tau) = \frac{\rho_0}{12\pi c^2}\frac{\partial^3}{\partial \tau^3}\int \frac{(\hat{\mathbf{x}}\cdot\mathbf{y})\mathbf{y}\cdot(\omega\times\hat{\mathbf{x}})}{|\mathbf{x}-\mathbf{y}|}\,\mathrm{d}V, \tag{4}$$

where the cadet denotes a unit vector, $\mathbf{y}$ the position of ω and V the volume of the vorticity-bearing fluid. The integral is evaluated at retarded time $t = \tau - |\mathbf{x}-\mathbf{y}|/c$.

The two-dimensional vortices produce a non-compact flow field. Their motions and the positions of their boundaries can be described by using the longitudinal and transverse co-ordinates, denoted thereinafter as y_1 and y_2 respectively (Figure 1). The spanwise direction y_3 is important only in the evaluation of the final farfield pressure fluctuations as the integral in equation (4) has to be taken over this dimension from $-\infty$ to $+\infty$ [20]. It is assumed that the farfield distance $|\mathbf{x}|$ is much larger than any length scale in the flow field and thus, the effect of vortex separation on the far field can be ignored. One should note that the present theory applies only to the cases where the vortex separation and vortex core size are both much smaller than the wavelength of sound radiated. The effect of source non-compactness found by Mitchell *et al.* [21] and the sound-flow interaction [2] can be neglected.

Denoting the cross-sectional area of the vortex system by A, equation (4) becomes

$$p(\mathbf{x}, \tau) = \frac{\rho_0}{12\pi c^2} \int_{-\infty}^{\infty} \frac{1}{|\mathbf{x} - \mathbf{y}|} \frac{\partial^3}{\partial t^3} \left(\cos 2\theta \oint \omega y_1 y_2 \, \mathrm{d}A + \sin 2\theta \oint \frac{y_2^2 - y_1^2}{2} \omega \, \mathrm{d}A \right) \mathrm{d}y_3, \quad (5)$$

showing that there are two quadrupoles co-existing. Equation (5) can be numerically integrated through a transformation to a time integration [14, 22]. However, such integration is not related to the sound generation mechanisms. The present study focuses the attention on the two source terms on the right-hand side of equation (5):

$$S_1 = \oint \omega y_1 y_2 \, \mathrm{d}A \quad \text{and} \quad S_2 = \frac{1}{2} \oint (y_2^2 - y_1^2) \omega \, \mathrm{d}A. \quad (6)$$

Since the steady motion of vorticity is not a source of sound, the effects of any mean motions in the two source terms have to be eliminated so they are not contributing to the final sound field. By defining the vorticity centroid of the vortex system $\mathbf{y}_{sc}$ as

$$\mathbf{y}_{sc} = \oint \omega y \, \mathrm{d}A \Big/ \oint \omega \, \mathrm{d}A, \quad (7)$$

where the integration is carried out over the cross-section of the vortex system and suppose this vortex system centroid $\mathbf{y}_{sc}$ is moving with a mean velocity of $\mathbf{U}(= U_1 \hat{y}_1 + U_2 \hat{y}_2)$, one can then define the relative position of a point inside the vortex core, $\mathbf{y}'$, such that $\mathbf{y}' = \mathbf{y} - \mathbf{y}_{sc} = \mathbf{y} - \mathbf{U}t$. Thus,

$$S_1 = \oint \omega y_1 y_2 \, \mathrm{d}A = \oint \omega (y_1' + U_1 t)(y_2' + U_2 t) \, \mathrm{d}A$$

$$= \oint \omega y_1' y_2' \, \mathrm{d}A + U_1 t \oint \omega y_2' \, \mathrm{d}A + U_2 t \oint \omega y_1' \, \mathrm{d}A + U_1 U_2 t^2 \oint \omega \, \mathrm{d}A, \quad (8a)$$

and

$$S_2 = \frac{1}{2} \oint \omega (y_2^2 - y_1^2) \, \mathrm{d}A$$

$$= \frac{1}{2} \oint \omega (y_2'^2 - y_1'^2) \, \mathrm{d}A + U_2 t \oint \omega y_2' \, \mathrm{d}A - U_1 t \oint \omega y_1' \, \mathrm{d}A + \frac{U_2^2 - U_1^2}{2} t^2 \oint \omega \, \mathrm{d}A. \quad (8b)$$

The integral $\oint \omega y_i' \mathrm{d}A$ $(i = 1, 2)$ vanishes according to the definition of y' and equation (7) provided that $\oint \omega \, \mathrm{d}A \neq 0$. Therefore, the last three terms on the right-hand side of equation (8) vanish after the triple time differentiation (equation (5)). The source strengths of the two quadrupoles are

$$\frac{\partial^3 S_1}{\partial t^3} = \frac{\partial^3}{\partial t^3} \oint \omega y_1' y_2' \, \mathrm{d}A \quad \text{and} \quad \frac{\partial^3 S_2}{\partial t^3} = \frac{1}{2} \frac{\partial^3}{\partial t^3} \oint (y_2'^2 - y_1'^2) \omega \, \mathrm{d}A. \quad (9)$$

Equation (9) contains no effect from the mean motion of the vortex interaction system, $\mathbf{U}$, and the quantities involved are all Galilean invariants. It is basically a generalized form of the theoretical deduction of Tang and Ko [14] for a steadily convecting vortex system.

By focusing on one of the interacting vortices and further defining $\mathbf{y}'' = \mathbf{y}' - \mathbf{y}_c$, where $\mathbf{y}_c$ denotes the vorticity centroid of the vortex concerned relative to the mean vortex interaction system motion,

$$\oint \omega y_1' y_2' \, \mathrm{d}A = \oint \omega y_1'' y_2'' \, \mathrm{d}A + y_{c1} \oint \omega y_2'' \, \mathrm{d}A + y_{c2} \oint \omega y_1'' \, \mathrm{d}A + y_{c1} y_{c2} \oint \omega \, \mathrm{d}A \tag{10a}$$

and

$$\frac{1}{2} \oint \omega (y_2'^2 - y_1'^2) \, \mathrm{d}A = \frac{1}{2} \oint \omega (y_2''^2 - y_1''^2) \, \mathrm{d}A + \sum_{i=1}^{2} (-1)^i y_{ci} \oint \omega y_i'' \, \mathrm{d}A + \frac{y_{c2}^2 - y_{c1}^2}{2} \oint \omega \, \mathrm{d}A, \tag{10b}$$

where the integrals have taken over the core of the vortex concerned. Since $\oint \omega y_i'' \, \mathrm{d}A = 0$, it follows that there are only two mechanisms through which vortex sound can be generated. The first one is the dynamics of the vorticity centroid of each vortex (terms involving $\mathbf{y}_c$ in equation (10)) and the second one is related to the unsteady motion of the core fluid relative to this centroid (terms involving $\mathbf{y}''$ in equation (10)). It will be shown later that the latter is strongly associated with the core deformation. Equations (9) and (10) are in general applicable to any two-dimensional vortex systems.

The results of Tang and Ko [14] have shown that the vorticity centroids of the interacting vortices are undergoing a nominal circular motion about the origin. The polar co-ordinate system, thus, appears more appropriate in describing their motions. Suppose the radius of the orbit of centroid motion is r_c, then

$$y_{c1} = r_c \cos\phi \quad \text{and} \quad y_{c2} = r_c \sin\phi, \tag{11}$$

where ϕ is the angular displacement of the vorticity centroid concerned. The source terms due to the vortex centroid dynamics become

$$S_1 = r_c^2 \cos\phi \sin\phi \oint \omega \, \mathrm{d}A \quad \text{and} \quad S_2 = \frac{1}{2} r_c^2 (\sin^2\phi - \cos^2\phi) \oint \omega \, \mathrm{d}A. \tag{12}$$

It can be observed that S_1 and S_2 have the same amplitudes but are 90° out of phase. The sound source strength resulting from this dynamics is, according to equation (9), given by

$$\frac{1}{2} \frac{\partial^3}{\partial t^3} \left(r_c^2 \oint \omega \, \mathrm{d}A \sin(2(\phi - \theta)) \right)$$

instead of the one having two components in equation (5). Since θ is a time invariant, it follows that the sound from the vorticity centroid dynamics is produced by the triple rate of change of the term, S_{polar}, where

$$S_{polar} = \frac{1}{2} r_c^2 \oint \omega \, \mathrm{d}A \sin(2\phi). \tag{13}$$

This is essentially S_1, showing that the source terms S_1 and S_2 are resulting from the same mechanism.

Since the cross-terms between the vorticity centroid dynamics and the microscopic fluid motions in the sound source terms vanish (equation (10)), the analysis of the sound production due to the fluid motions relative to the centroid can be done in exactly the same

way as discussed above. The corresponding source term S'' is

$$S'' = \frac{1}{2}\oint \omega r''^2 \sin(2(\phi'' - \theta))\,\mathrm{d}A, \tag{14}$$

where $''$ denotes quantity relative to the vorticity centroid of the vortex core concerned. Suppose the core boundary relative to this vorticity centroid is defined by a curve $\xi(\phi'')$, then

$$S'' = \frac{\omega}{2}\int_0^{2\pi}\int_0^{\xi} r''^3 \sin(2(\phi'' - \theta)\,\mathrm{d}r''\,\mathrm{d}\phi'' = \frac{\omega}{8}\int_0^{2\pi} \xi^4(\phi'')\sin(2(\phi'' - \theta))\,\mathrm{d}\phi''. \tag{15}$$

S'' is zero if the vortex core is circular and is a constant if the core shape is non-circular but remains unchanged relative to the vorticity centroid. This shows explicitly that the sound field resulted from the fluid motions relative to the vorticity centroid (equation (10)) is related to the unsteady vortex core deformation during the vortex interaction.

3. NUMERICAL RESULTS AND DISCUSSIONS

3.1. IDENTICAL VORTICES

3.1.1. *Leapfrogging*

The initial vortex cores of the present study are taken to be circular. Figure 2 shows a typical example of the vortex motion for $G/\sigma = 6$, where G and σ are the vorticity centroid

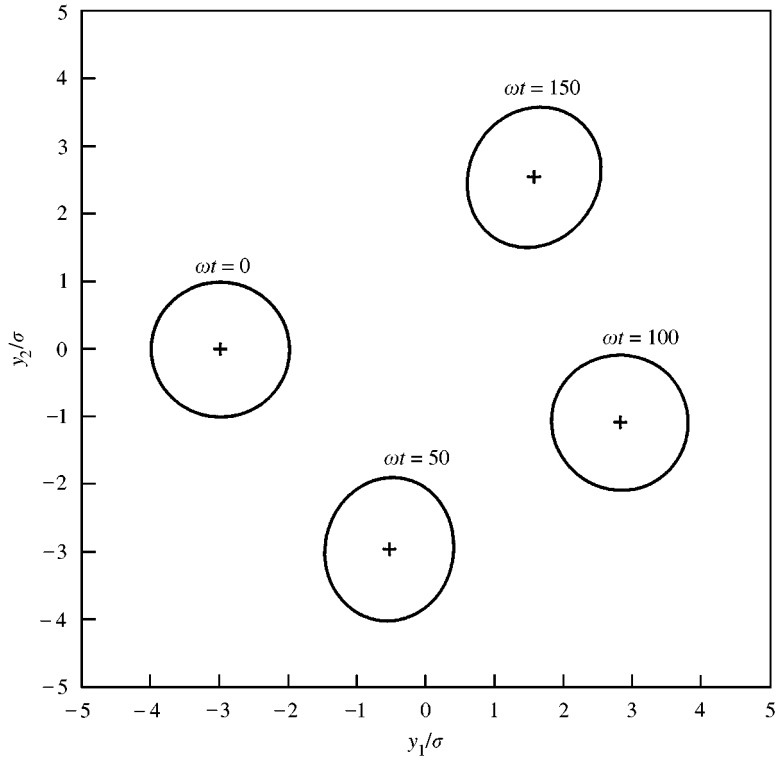

Figure 2. Identical vortex core evolution. $G/\sigma = 6$: ——, core boundary; +, vorticity centroid.

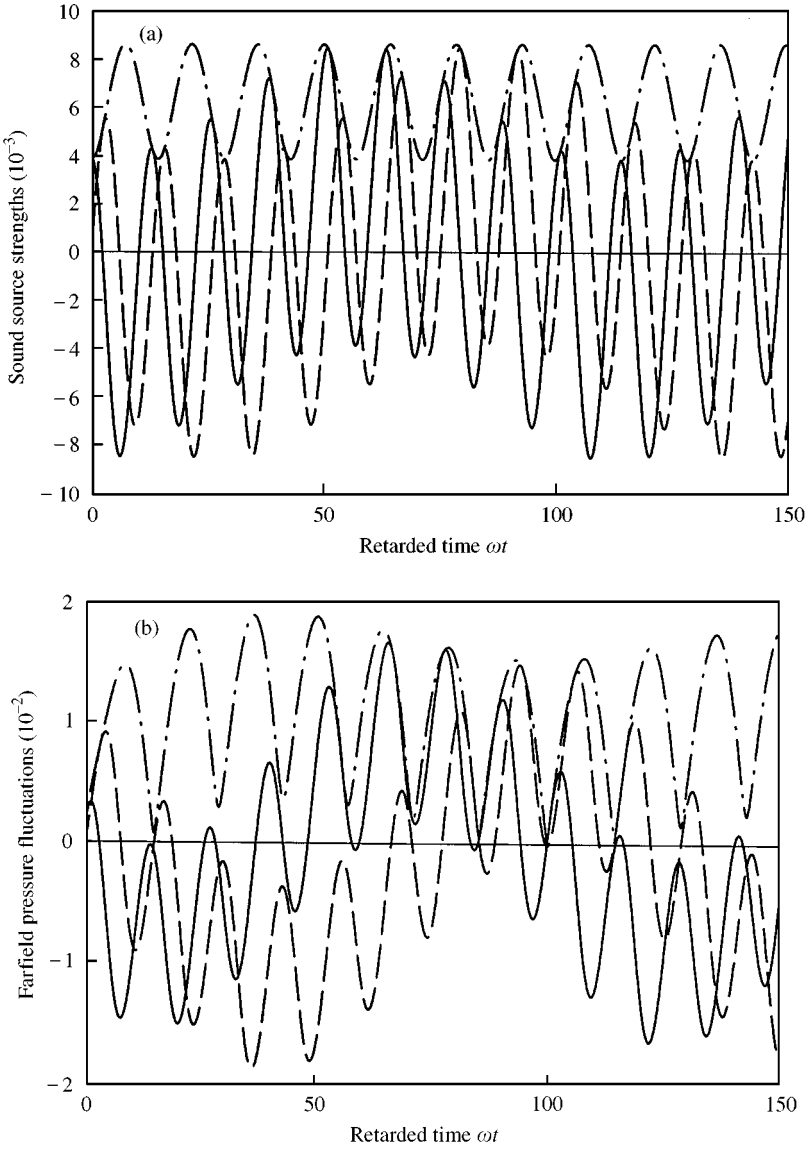

Figure 3. (a) Time variations of source strengths under leapfrogging vortex motion: ——, $\partial^3 S_1/\partial t^3$; — —, $\partial^3 S_2/\partial t^3$; —·—, source strength magnitude. (b) Time variations of farfield pressure under leapfrogging vortex motion: ——, from $\partial^3 S_1/\partial t^3$; — —, from $\partial^3 S_2/\partial t^3$; —·—, pressure magnitude. $G/\sigma = 6$.

initial separation and the initial core radius respectively (Figure 1). Only one vortex core is shown as the other is just the mirror image in the opposite quadrant. The two vortices rotate about the origin with some core deformations. The time variations of the corresponding sound source strengths, $\partial^3 S_1/\partial t^3$ and $\partial^3 S_2/\partial t^3$ (equation (9)), are given in Figure 3(a). The source strengths contain two major components—one of low frequency and the other of higher frequency. Figure 3(b) shows the farfield pressure fluctuations obtained after performing the integration in equation (5). The results show that the integration has only reduced the magnitudes of the high-frequency components relative to

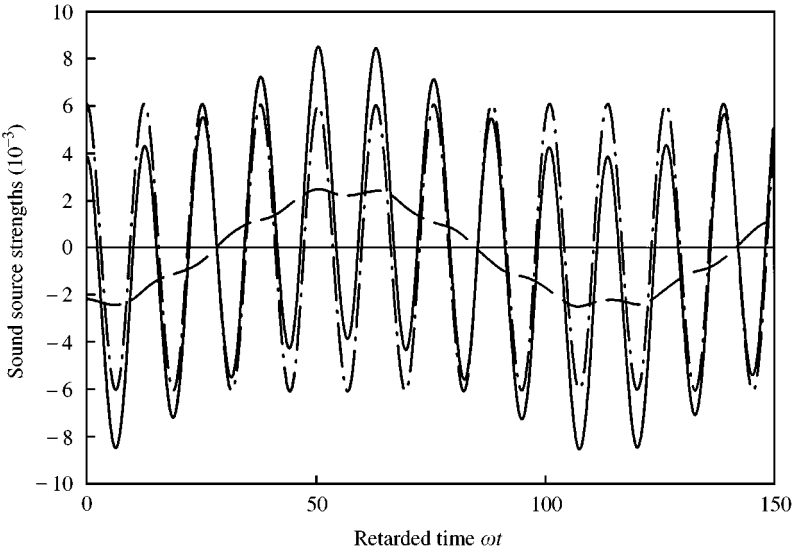

Figure 4. Decomposition of $\partial^3 S_1/\partial t^3$. $G/\sigma = 6$: ——, $\partial^3 S_1/\partial t^3$; — —, $\partial^3 S_{polar}/\partial t^3$; —·—, $\partial^3 S''/\partial t^3$.

the low-frequency ones; an observation similar to that found by Tang and Ko [14]. The decomposition of the source terms (equation (10)) shows that the low-frequency component is generated by the vorticity centroid dynamics, while the higher frequency one is produced by the terms associated with the fluid motions relative to the vorticity centroids (Figure 4).

Similar high-frequency farfield pressure fluctuations are also observed by Shariff *et al.* [23] for vortex ring interaction. Shariff *et al.* [23] also ascribed that such fluctuations are the results of core rotation and notation. However, such fluctuations are not found in the results of the direct computations of Mitchell *et al.* [21]. The reason for this is not known, but it has been found that the increase in the bulkiness of vortex cores reduces the magnitudes of the high-frequency farfield pressure fluctuations [13]. The compressibility and viscosity of a real fluid may also tend to damp down the high-frequency fluid motions within the vortex cores. This issue is left to further investigation.

The circulation of each vortex does not change with time. One can then decompose the triple time derivative of S_{polar}, as depicted in equation (13), in the same way as in Tang and Ko [12] with an understanding that the farfield observer angle θ is ignored:

$$\frac{\partial^3 S_{polar}}{\partial t^3} = \frac{1}{2}\oint \omega \, \mathrm{d}A \left(\sin(2\phi) \frac{\partial^3 r_c^2}{\partial t^3} + 3 \frac{\partial^2 r_c^2}{\partial t^2} \frac{\partial \sin(2\phi)}{\partial t} + 3 \frac{\partial r_c^2}{\partial t} \frac{\partial^2 \sin(2\phi)}{\partial t^2} + r_c^2 \frac{\partial^3 \sin(2\phi)}{\partial t^3} \right). \tag{16}$$

It should be noted that the time variation of r_c, though of a very small magnitude, contains a component having frequency the same as those of the high-frequency fluctuations in the source strengths presented in Figure 4. However, it can be shown that the last term on the right-hand side of equation (16) contributes substantially to the sound generation. A further decomposition of this term suggests

$$\frac{\partial^3 S_{polar}}{\partial t^3} \approx -4\cos(2\phi) r_c^2 \dot{\phi}^3 \oint \omega \, \mathrm{d}A + R, \tag{17}$$

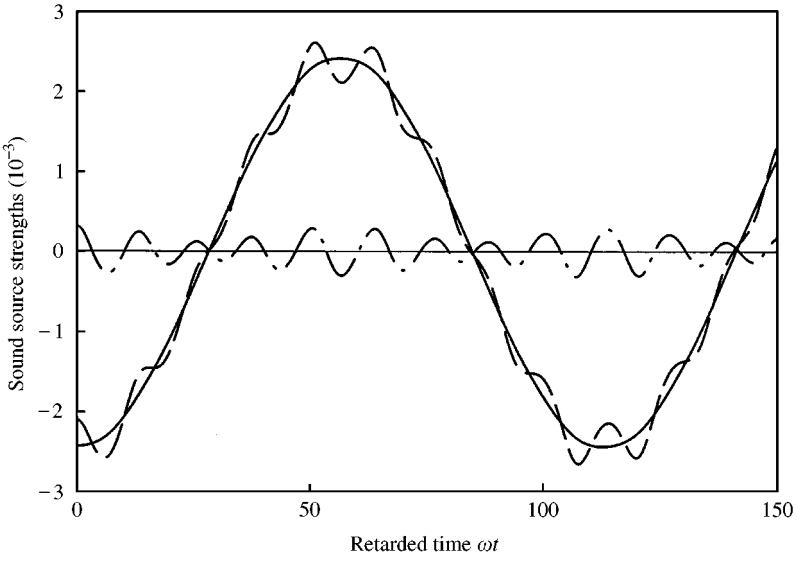

Figure 5. Decomposition of $\partial^3 S_{polar}/\partial t^3$. $G/\sigma = 6$: ——, $-4\cos(2\phi) r_c^2 \dot{\phi}^3 \omega \, \mathrm{d}A$; — —, $\partial^3 S_{polar}/\partial t^3$; —·—, R.

where $\dot{\phi} = \partial\phi/\partial t$ and R is the remainder. The latter varies nearly sinusoidal with time (Figure 5). However, the magnitude of R is insignificant when compared to those of the high-frequency fluctuations associated with the fluid motions relative to the vorticity centroid.

If one assumes no deformation of vortex core so that the core remains circular throughout the interaction, the overall effects of the fluid motions relative to the vorticity centroid on sound generation vanish, that is, $\partial^3 S''/\partial t^3 = 0$. Also, $R \equiv 0$ when $\dot{\phi}$ and r_c are constants. Equation (17) is then the spinning vortex sound of Powell [3]. In addition, the expression $r_c^2 \oint \omega \, \mathrm{d}A$ represents the angular momentum of the vortex system if the vortex cores remain circular. Since the total angular momentum of each vortex is conserved even if core deformation takes place, R can be interpreted as the generation of sound due to a transfer of the angular momentum between the macroscopic mean motion and the microscopic core fluid activities. However, this component is not important as illustrated in Figure 5.

Figure 4 and equation (14) show that the higher frequency component in the sound source strength is due to the unsteady core deformation. The magnitude of the source strength $|\partial^3 S''/\partial t^3|$ varies slightly with time (Figure 6). Figure 7 shows the core shapes of the vortex at $\omega t = 86$ and 92·4, corresponding to the instants of maximum and minimum source strength magnitudes respectively. The highest source strength appears at the instant when the vortex core is approximately circular. In order to get a deeper insight into the relationship between core deformation and the source strength magnitude, core deformation here is defined by using a differential radius

$$\Delta\sigma = \pm (\max|\mathbf{y} - \mathbf{y}_c| - \min|\mathbf{y} - \mathbf{y}_c|). \tag{18}$$

The "+" and "−" signs denote the circumstances when the longer principal axis is in the first/third and second/fourth quadrants respectively. The rate of core deformation is, therefore, $\partial(\Delta\sigma)/\partial t$. Figure 8 shows clearly that a higher source strength magnitude is associated with a higher rate of core deformation. The rate of deformation is the highest at the instant when the vortex core is circular ($\Delta\sigma = 0$). The same phenomenon is observed in

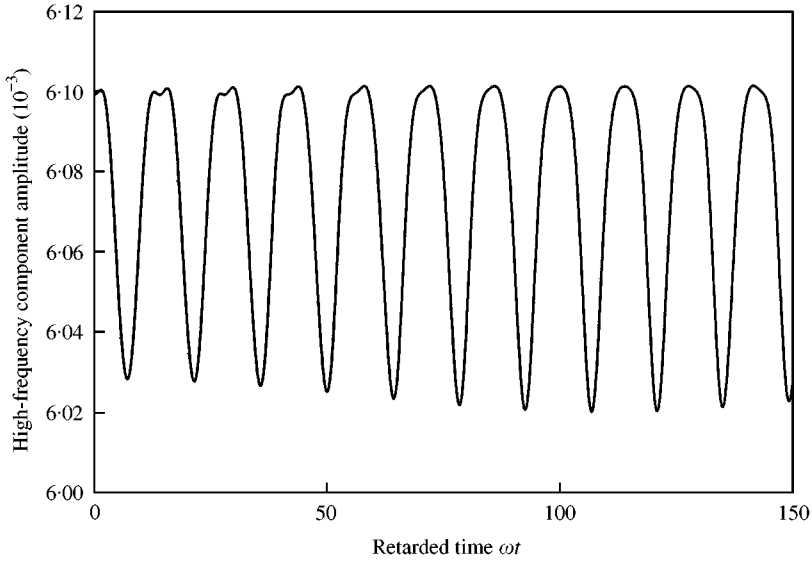

Figure 6. Time variation of $\partial^3 S''/\partial t^3$ magnitude. $G/\sigma = 6$.

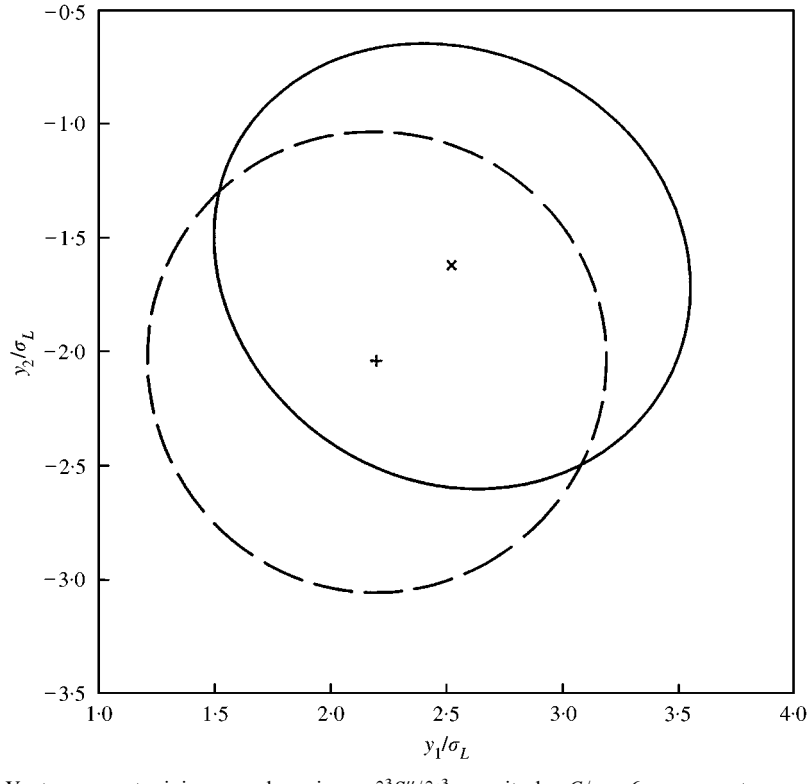

Figure 7. Vortex cores at minimum and maximum $\partial^3 S''/\partial t^3$ magnitudes. $G/\sigma = 6$: — —, vortex core at $\omega t = 86$; ——, vortex core at $\omega t = 92{\cdot}4$; +, vorticity centroid at $\omega t = 86$; ×, vorticity centroid at $\omega t = 92{\cdot}4$.

the leapfrogging motion of two-dimensional vortices at other G/σ (not shown here). The smaller this separation, the larger the core deformation and source strength magnitude time fluctuation.

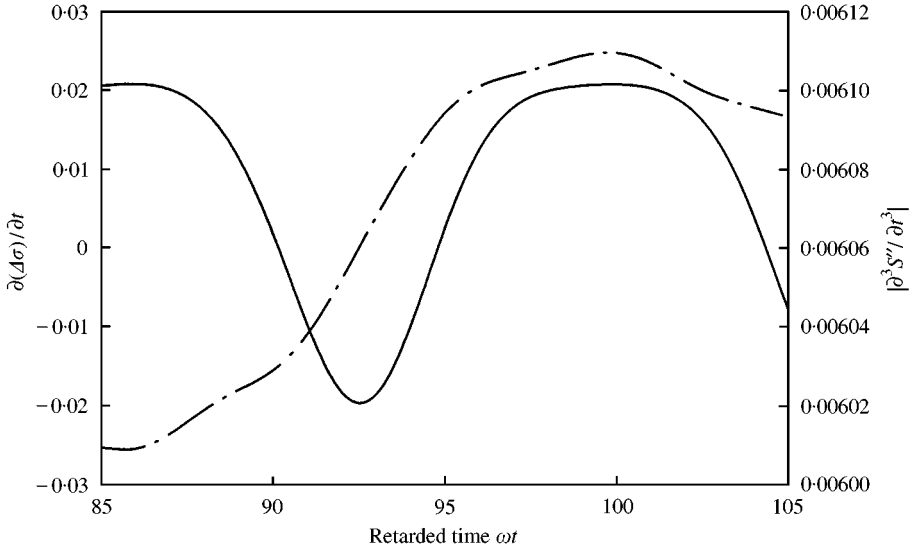

Figure 8. Relationship between $\partial^3 S''/\partial t^3$ magnitude and core deformation rate. $G/\sigma = 6$. ——, $|\partial^3 S''/\partial t^3|$; —·—, $\partial(\Delta\sigma)/\partial t$.

The source strength of the high-frequency component $\partial^3 S''/\partial t^3$ cannot be decomposed as in equation (16). Since Figure 2 shows that the vortex cores are approximately elliptical, one can assume that each vortex core is a tilted ellipse such that

$$\xi(\phi'') = \sqrt{a_1^2 \cos^2(\phi'' - \beta) + a_2^2 \sin^2(\phi'' - \beta)}, \tag{19}$$

where β is the tilt angle, a_1 and a_2 are the half-length of the longer and shorter principal axis respectively ($a_1 \geqslant a_2$). Then equation (15) gives

$$S'' = \frac{\pi\omega}{32}(a_1^4 - a_2^4)\sin(2(\beta - \theta)) = \frac{\Gamma}{16}(a_1 + a_2)(a_1 - a_2)\sin(2(\beta - \theta)). \tag{20}$$

When the longer principal axis of the core is in the first/third quadrant, $\sin(2\beta)$ is positive. The reverse is true when this axis is in the other two quadrants. The sound so produced is highly related to the rate of change of the difference $(a_1 - a_2)$ and the rotation of the vortex core principal axes. The deduction from this elliptical core assumption appears consistent with equation (18) and with the results shown in Figures 6 and 8.

In this case of $G/\sigma = 6$, the term $(a_1 + a_2)$ varies less than 0·3% (not shown here). One can then conclude that

$$\frac{\partial^3 S''}{\partial t^3} \propto \frac{\partial^3}{\partial t^3}((a_1 - a_2)\sin(2(\beta - \theta))). \tag{21}$$

Figure 9 shows clearly the validity of this elliptical core analysis, though there is a small discrepancy between the magnitudes of the actual S'' (equation (14)) and that estimated by the elliptical core assumption (equation (20)). The frequency of source term fluctuations is the same. This is acceptable, as the cores are not exactly elliptical. This confirms that the source of high-frequency source strength fluctuations is the coupling between the rate of core deformation and the rotation of the core relative to the vorticity centroid. Further decomposition of equation (21), as in equation (16), is not possible as the factor $(a_1 - a_2)$ is

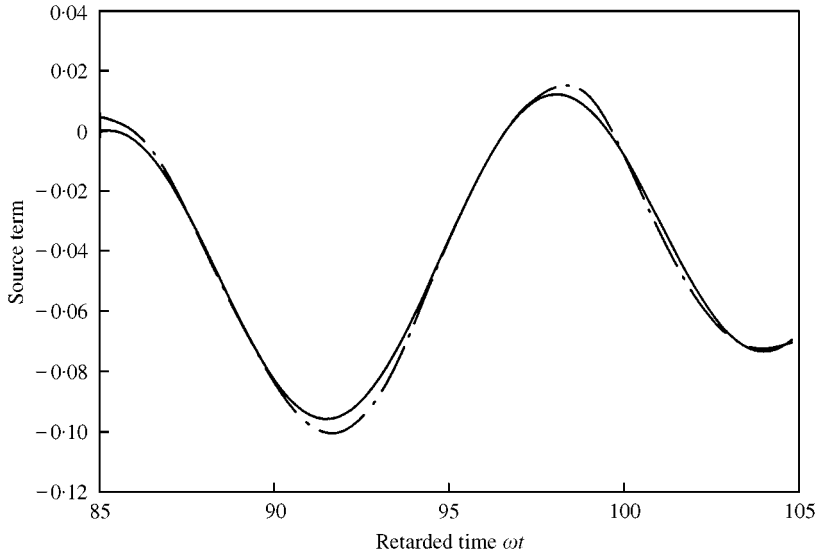

Figure 9. S'' compared to that from elliptical core assumption. $G/\sigma = 6$, $\theta = 0$: ——, S''; —·—, elliptical core assumption.

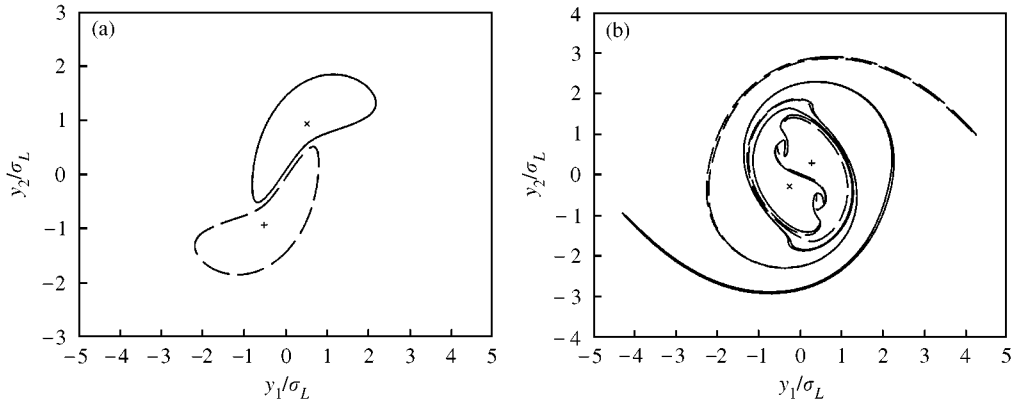

Figure 10. Vortex core evolution under coalescence. $G/\sigma = 2{\cdot}5$. (a) $\omega t = 6{\cdot}1$; (b) $\omega t = 40$: ——, — —, core boundaries; +, ×, vorticity centroids.

not time differentiable at the instant when the core becomes circular (thus, $a_1 = a_2$). Similar results are obtained for other G/σ, in which the leapfrogging vortex motions are observed (not shown here).

3.1.2. *Coalescence*

Since the vortex boundary cannot come into mutual contact in the inviscid model, coalescence is defined as the mutual "folding together" of two interacting finite areas of non-zero vorticity, as in Jacobs and Pullin [24]. Two vortices coalesce with each other when G/σ is sufficiently small. A typical example with $G/\sigma = 2{\cdot}5$ is shown in Figure 10.

Figure 11(a) shows the time variations of the source strengths and the overall source amplitude. Unlike the leapfrogging case, the source amplitude increases to a maximum at

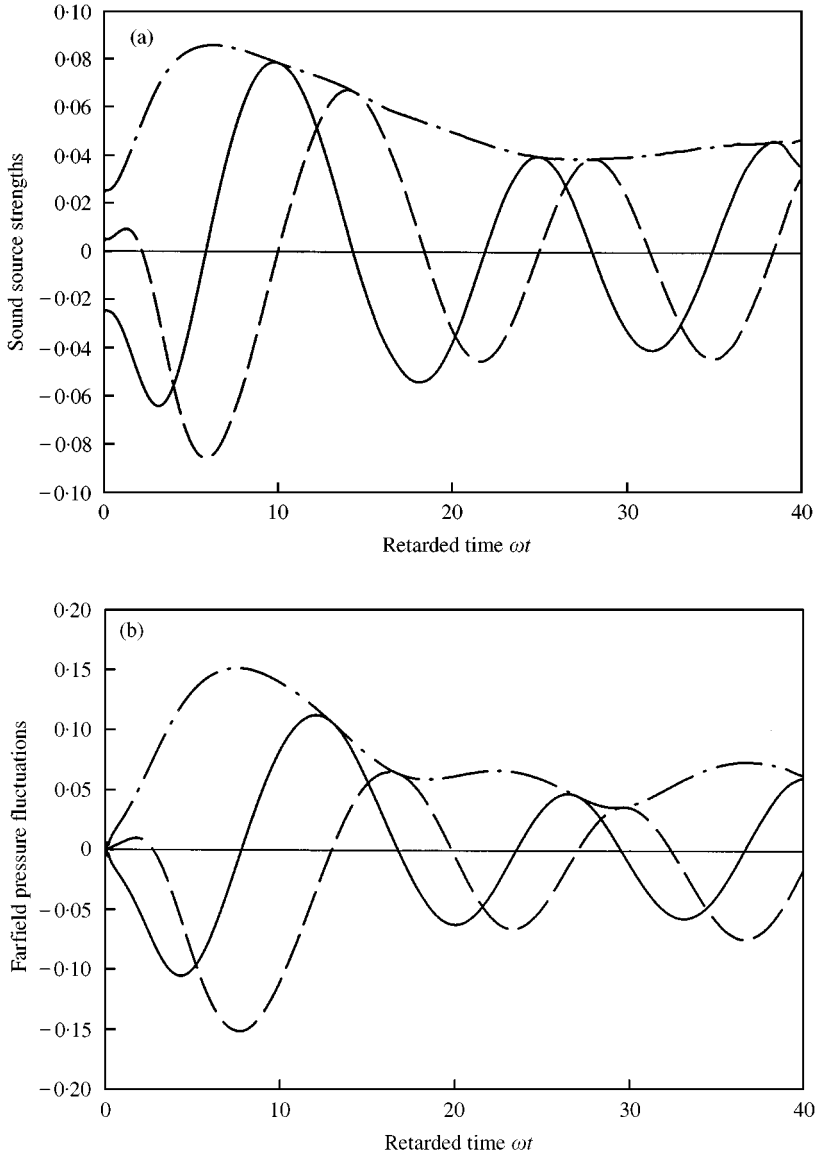

Figure 11. (a) Time variations of source strengths under vortex coalescence: ——, $\partial^3 S_1/\partial t^3$; — —, $\partial^3 S_2/\partial t^3$; —·—, source strength magnitude. (b) Time variations of farfield pressure under vortex coalescence: ——, from $\partial^3 S_1/\partial t^3$; — —, from $\partial^3 S_2/\partial t^3$; —·—, pressure magnitude. $G/\sigma = 2{\cdot}5$.

$\omega t \approx 6{\cdot}1$ and no sinusoidal fluctuation is found afterward. Maximum source strength amplitude is observed during the first "folding up" of the vortex cores, at which the cores become substantially "L" shaped (Figure 10(a)). It can also be noted from Figures 4 and 11(a) that the magnitude of the source strength produced by vortex coalescence is higher than that by the leapfrogging vortex motions. This is probably due to the higher energy content of the present coalescing vortex system, which leads to a more unsteady and rigorous vortex interaction. Figure 11(b) shows the farfield pressure fluctuation time variations obtained after the integration in equation (5). They are similar to those shown in Figure 11(a) and thus are not discussed.

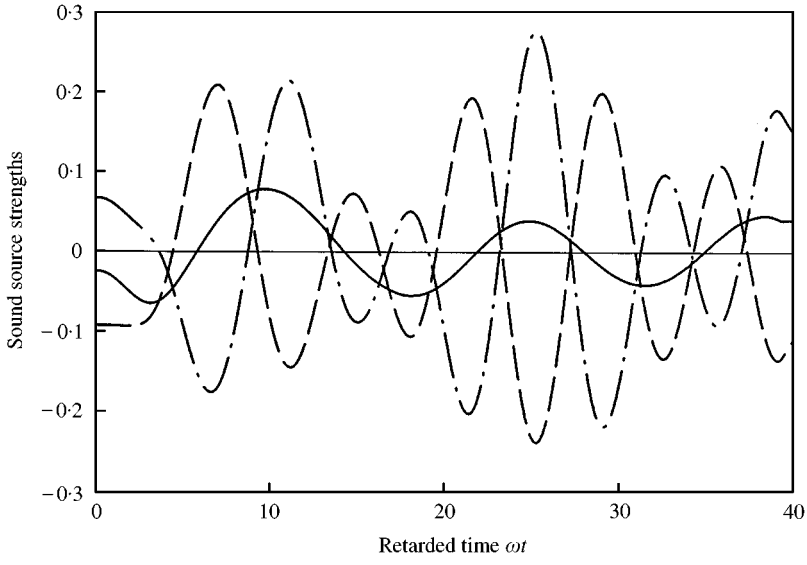

Figure 12. Decomposition of $\partial^3 S_1/\partial t^3$. $G/\sigma = 2{\cdot}5$: ——, $\partial^3 S_1/\partial t^3$; — —, $\partial^3 S_{polar}/\partial t^3$; —·—, $\partial^3 S''/\partial t^3$.

Since it has been shown previously that the source terms S_1 and S_2 from the same mechanisms, the following discussions will focus on S_1 only. The time variations of the source strengths due to the vorticity centroid dynamics and unsteady core deformation are illustrated in Figure 12. These fluctuations contain high-frequency components, which tend to counteract each other. The resultant $\partial^3 S_1/\partial t^3$ is of lower frequency. This observation differs significantly from the results in the leapfrogging case, where the two mechanisms produce sound of different frequencies.

As the vortex cores are seriously deformed, the differential radius, as defined in equation (18), cannot be used and the integral for the core deformation source term S'' cannot be solved explicitly. However, one can observe from Figure 13 that the source strengths due to unsteady core deformation and vorticity centroid dynamics contain low- and high-frequency components. The low-frequency component has a frequency about half that of the high-frequency one. The strengths of the high-frequency components from these two mechanisms are the same and they are 180° out of phase (not shown here) such that the resultant $\partial^3 S_1/\partial t^3$ does not contain this frequency component (Figure 13). The energy level of the low-frequency component produced by the unsteady core deformation is 6 dB higher than that from the vorticity centroid dynamics. Together with their out-of-phase relationship, the resultant has an amplitude half that produced by the unsteady core deformation. The present result shows clearly that the final sound field generated by vortex coalescence is purely the result of the unsteady vortex core deformation.

The time variation of $\mathbf{y}_c$ of one of the vortex cores shows good correlation with $\partial^3 S_1/\partial t^3$ and $\partial^3 S_2/\partial t^3$, except at short period at the beginning of the interaction (Figure 14). Taking $\partial^3 S_1/\partial t^3$ as an example, the source strength peaks at $\omega t = 9{\cdot}66$, 24·8 and 38·4, while the corresponding troughs are found at $\omega t = 3$, 18 and 31·4. The core shapes at these instants are shown in Figure 15. The peaks of $\partial^3 S_1/\partial t^3$ are observed when the majority of the core fluid of the vortex initially at $y_1 < 0$ is on the positive y_1-axis and they appear in every cycle when the thin vortex core tail wraps round its main core (c.f. Figure 15(d) and 15(f)). The troughs are found when the majority of the core fluid of the same vortex is on the negative y_1-axis and their period is the same as that of the peaks. Similar phenomena are observed

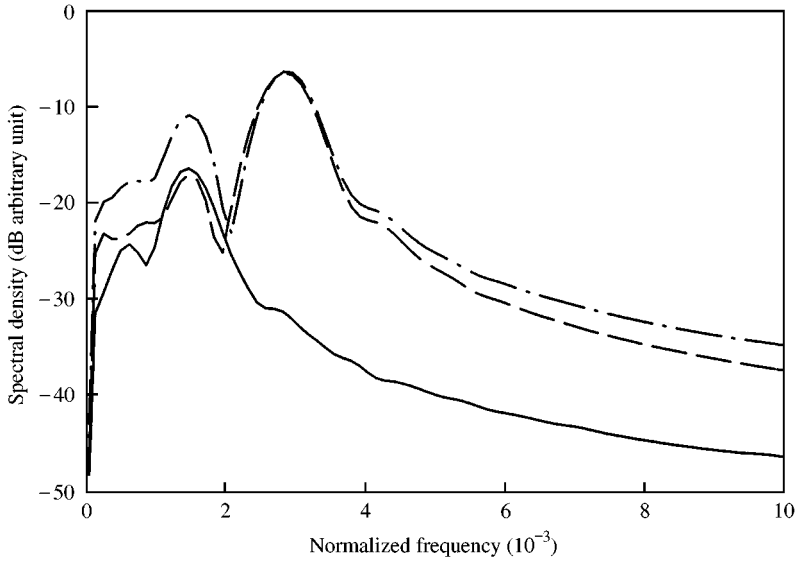

Figure 13. Frequency spectra of source strengths. $G/\sigma = 2{\cdot}5$: ——, $\partial^3 S_1/\partial t^3$; — —, $\partial^3 S_{polar}/\partial t^3$; —·—, $\partial^3 S''/\partial t^3$.

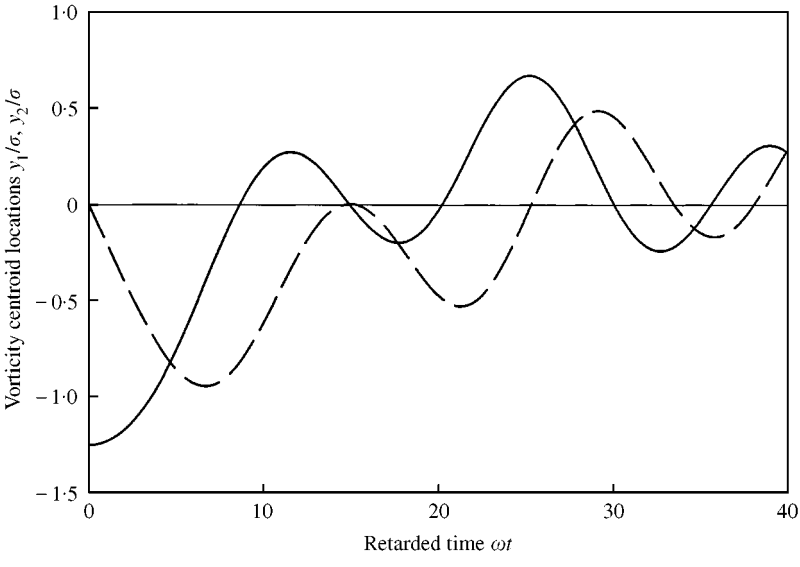

Figure 14. Time variations of vorticity centroid position at $G/\sigma = 2{\cdot}5$: ——, y_1/σ; — —, y_2/σ.

for $\partial^3 S_2/\partial t^3$, but the corresponding instants of peaks and troughs are related to the y_2-axis. The sound produced by vortex coalescence, therefore, depends on the rate of "folding together" between the vortices. However, since the core shapes are very irregular, a more explicit form of the source strength cannot be found.

Comparing with the data of $G/\sigma = 3$ of Tang and Ko [14], the source strengths in the present study ($G/\sigma = 2{\cdot}5$) are higher, showing that these strengths increase with increasing rate of vortex core "folding up".

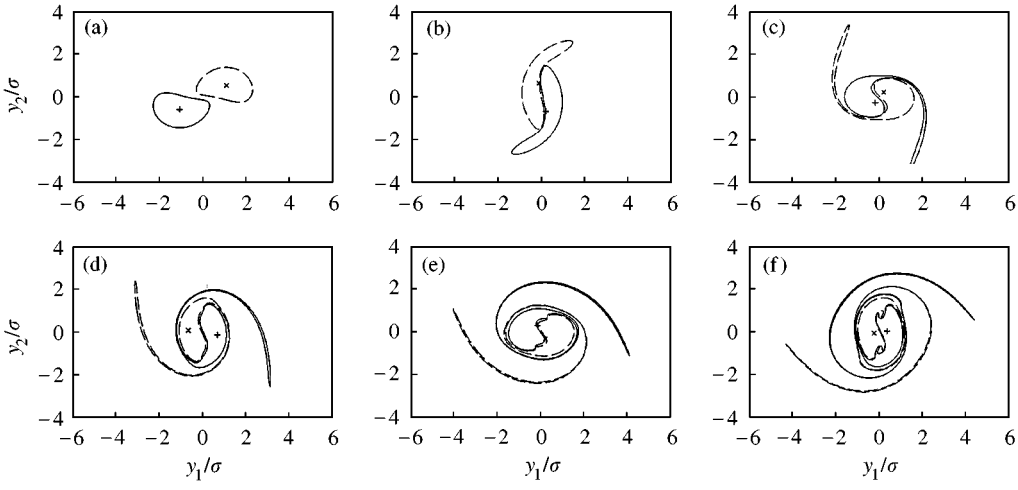

Figure 15. Vortex core shapes at crests and toughs of $\partial^3 S_1/\partial t^3$. $G/\sigma = 2{\cdot}5$: (a) $\omega t = 3$; (b) $\omega t = 9{\cdot}66$; (c) $\omega t = 18$; (d) $\omega t = 24{\cdot}8$; (e) $\omega t = 31{\cdot}4$; (f) $\omega t = 38{\cdot}4$: ——, — —, core boundaries; $+$, $\times$, vorticity centroids.

3.2. UNEQUAL VORTICES

3.2.1. *Leapfrogging*

Leapfrogging motion with mild core deformation also occurs when two vortices of different circulations interact (Figure 16). The vortices have the same vorticity ω, but the ratio of their initial diameter is 2 : 1, giving a circulation ratio of 4. The initial vorticity centroid separation G/σ_L is 5, where σ_L is the initial radius of the stronger vortex. Without loss of generality, the vortex initially on the negative y_1-axis is assumed to possess higher circulation. The suffices R and L thereinafter denote quantity associated with the weaker and stronger vortices respectively. Since the integration in equation (5), at the most, only reduces the importance of the high-frequency source strength fluctuations in the overall sound generation and is not related to any sound generation mechanism, it is not further performed.

The vorticity centroids undergo nominal circular motion about the centroid of the interacting system, which is at $y_1/\sigma_L = -1{\cdot}5$ and $y_2/\sigma_L = 0$. Similar to the identical vortex leapfrogging case, the time variations of their accelerations, jerks and velocities contain high-frequency components.

The source strengths of the two vortices are depicted in Figure 17. All of them contain high- and low-frequency sinusoid fluctuations. Again, the discussions on the sound generation mechanisms are focused on the source strengths $\partial^3 S_{1L}/\partial t^3$ and $\partial^3 S_{1R}/\partial t^3$. Basically, each of them consists of low- and high-frequency components (Figure 18). The low-frequency component in $\partial^3 S_{1R}/\partial t^3$ is stronger than that in $\partial^3 S_{1L}/\partial t^3$, but the opposite is observed for the high-frequency components. The results in Figure 18 suggest that the weaker and stronger vortices produce, respectively, the low- and high-frequency farfield sound.

As in the identical vortex case, the amplitude of the low-frequency sound depends on the third power of the vorticity centroid angular speed (not shown here). Equation (17) again applies to this case of unequal vortex leapfrogging motions. The high-frequency components in the source strengths are the results of unsteady vortex core deformation (S'') and rotation of core fluids about the associated vorticity centroids. Since the deformation of

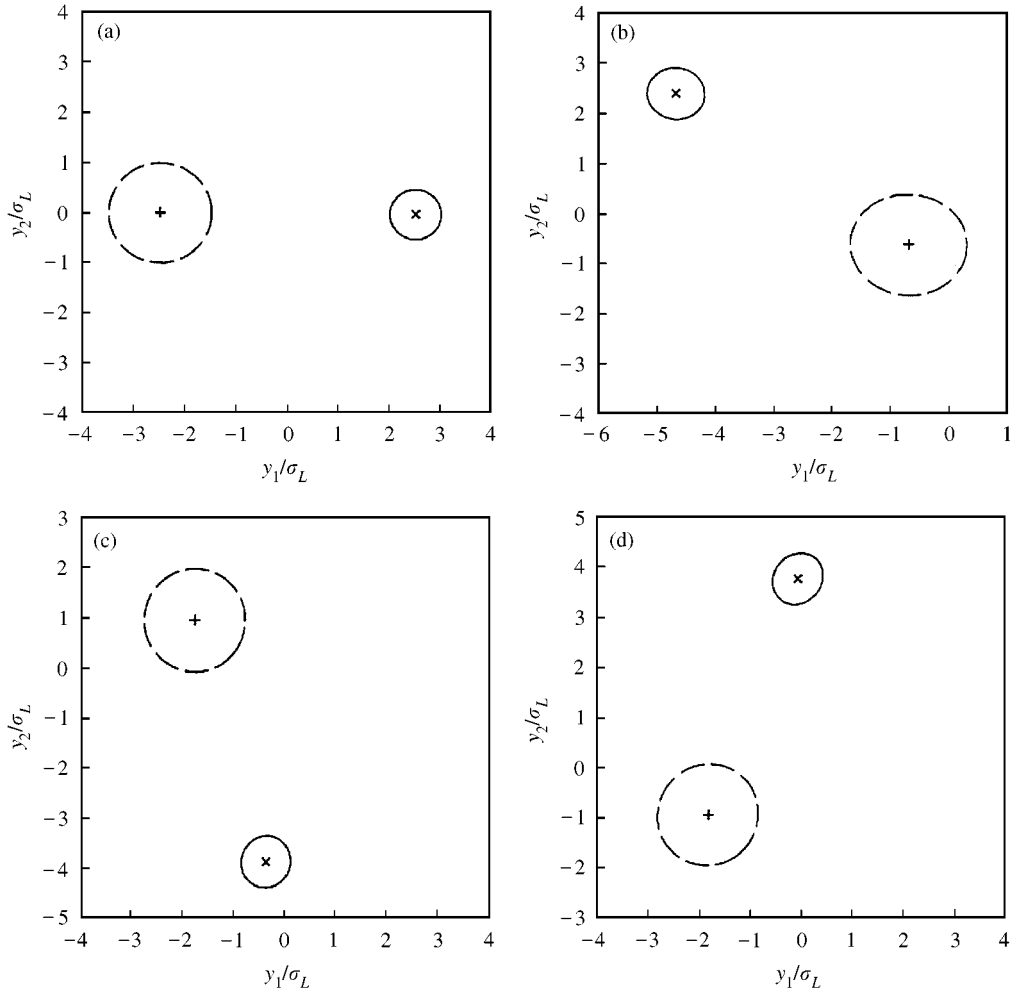

Figure 16. Core evolution under unequal vortex leapfrogging. $\Gamma_L/\Gamma_R = 4$, $G/\sigma_L = 5$, $\sigma_L/\sigma_R = 2$. (a) $\omega t = 0$; (b) $\omega t = 10$; (c) $\omega t = 20$; (d) $\omega t = 30$: ——, core boundary of stronger vortex; — —, core boundary of weaker vortex; +, vorticity centroid of stronger vortex, ×, vorticity centroid of weaker vortex.

vortex core is not significant, the elliptical core analysis in the identical vortex leapfrogging case is still valid. The corresponding results are very similar to those presented in Figure 9 and thus are not presented.

3.2.2. *Interaction at large circulation ratio*

When the circulation ratio between the two vortices increases, the weaker vortex is sheared into a vorticity strip under the induced velocity field of the stronger vortex. However, there is no mutual "folding together" of the vortex cores. An example of such a phenomenon with $\Gamma_L/\Gamma_R = 160$, $\sigma_L/\sigma_R = 2$ and $G/\sigma_L = 5$ is shown in Figure 19. The stronger vortex experiences slight deformation and its vorticity centroid is nearly at rest. The distance between the vorticity centroids decreases at increased interaction time.

The source strength fluctuations for the above interaction conditions (Figure 19) are illustrated in Figure 20. The contribution from the stronger vortex contains only

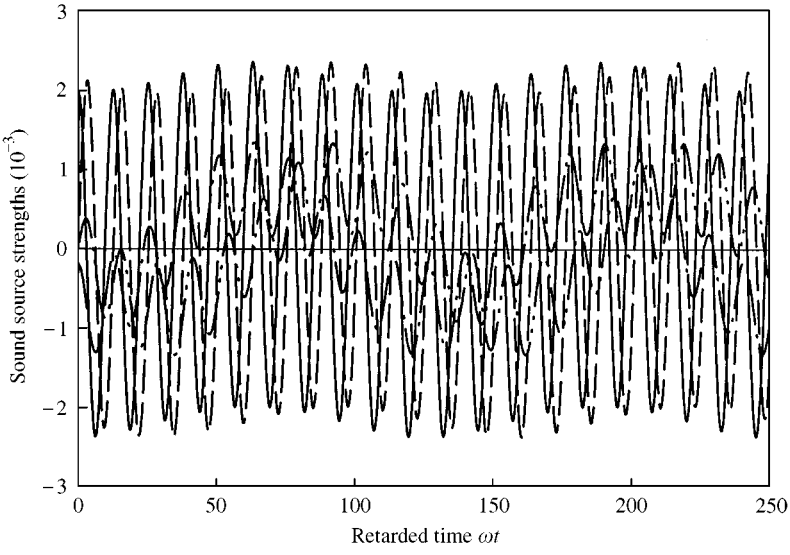

Figure 17. Time variations of source strengths. $\Gamma_L/\Gamma_R = 4$, $G/\sigma_L = 5$, $\sigma_L/\sigma_R = 2$:——, $\partial^3 S_1/\partial t^3$ of stronger vortex; — —, $\partial^3 S_2/\partial t^3$ of stronger vortex; —·—, $\partial^3 S_1/\partial t^3$ of weaker vortex; —··—, $\partial^3 S_2/\partial t^3$ of weaker vortex.

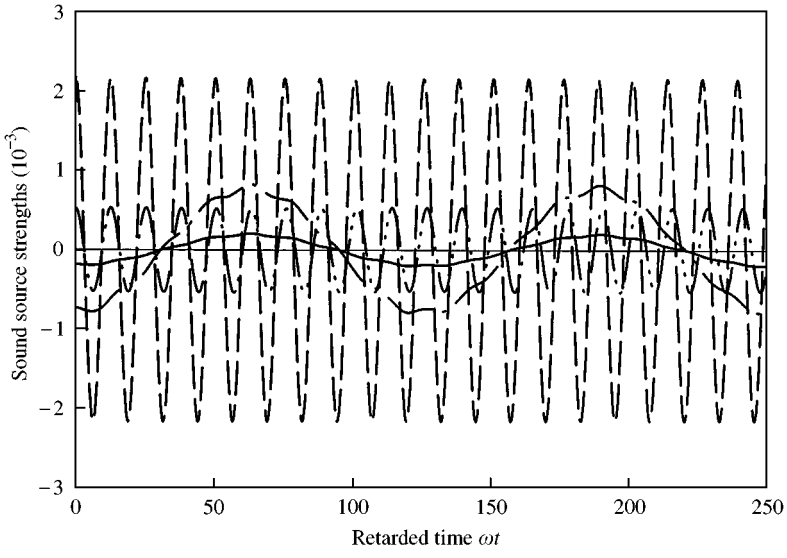

Figure 18. Decomposition of $\partial^3 S_1/\partial t^3$. $\Gamma_L/\Gamma_R = 4$, $G/\sigma_L = 5$, $\sigma_L/\sigma_R = 2$: ——, $\partial^3 S_{polar}/\partial t^3$ of stronger vortex; — —, $\partial^3 S''/\partial t^3$ of stronger vortex; —·—, $\partial^3 S_{polar}/\partial t^3$ of weaker vortex; —··—, $\partial^3 S''/\partial t^3$ of weaker vortex.

a high-frequency sinusoidal component, due to the small core deformation as discussed previously. The disappearance of the low-frequency component is due to the very weak motion of its centroid. The causes have been discussed previously.

The contribution from the weaker vortex is of low frequency which is approximately twice that of the rotational speed of the weaker vortex vorticity centroid relative to the centroid of the interacting system ($y_1/\sigma_L = -2{\cdot}469$, $y_2/\sigma_L = 0$). This tends to suggest that the dynamics of the vorticity centroid are responsible for the sound generation and equation (13) is appropriate in describing the underlying mechanism. Again, equation (17)

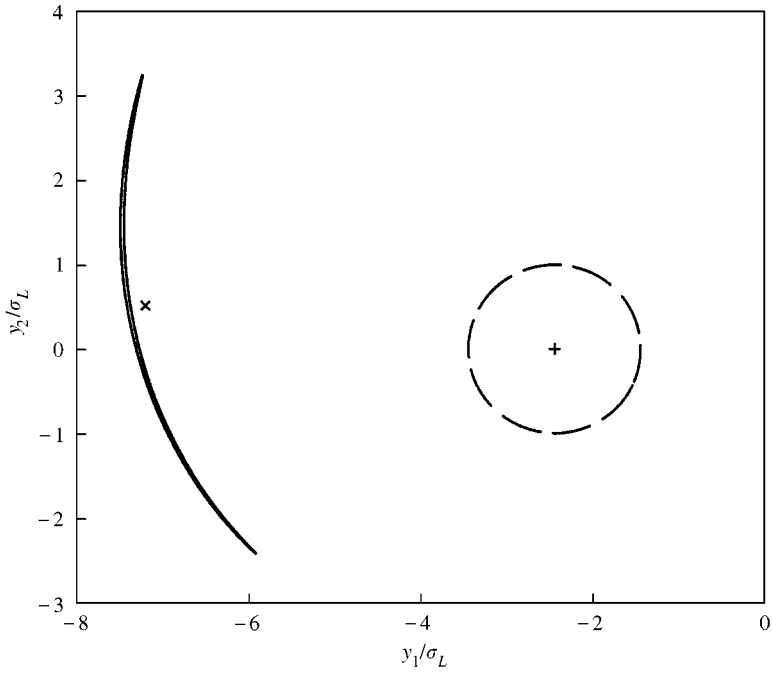

Figure 19. Vortex cores under larger circulation ratio. $\Gamma_L/\Gamma_R = 160$, $G/\sigma_L = 5$, $\sigma_L/\sigma_R = 4$: ——, core boundary of stronger vortex; — —, core boundary of weaker vortex; +, vorticity centroid of stronger vortex; ×, vorticity centroid of weaker vortex.

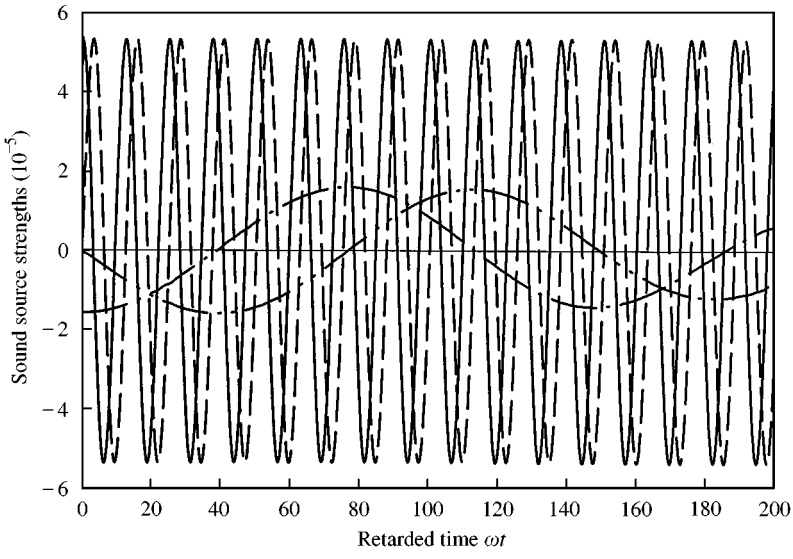

Figure 20. Time variations of source strengths. $\Gamma_L/\Gamma_R = 160$, $G/\sigma_L = 5$, $\sigma_L/\sigma_R = 4$. Legends: same as those in Figure 17.

is valid and the remainder R in this case is small (Figure 21). A further decomposition of the remainder R suggests that the term $\Gamma_R(\partial r_c^2/\partial t)(\partial^2 \sin 2\phi/\partial t^2)$ contributes to a major part of R at increased interaction time (Figure 21). Since the angular speed of the vorticity centroid in this case is nearly time invariant, the magnitude of this term is related approximately to the Corollis acceleration discussed by Doak [5].

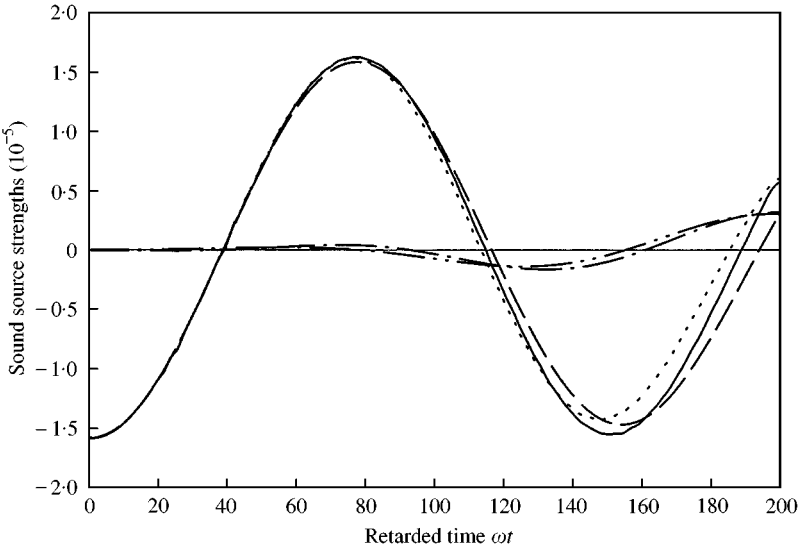

Figure 21. Decomposition of weaker vortex contribution. $\Gamma_L/\Gamma_R = 160$, $G/\sigma_L = 5$, $\sigma_L/\sigma_R = 4$:— —, $-4\Gamma_R \cos(2\phi) r_c^2 \dot{\phi}^3$; ——, $\partial^3 S_{polar}/\partial t^3$; —·—, R; ·····, $\partial^3 S_1/\partial t^3$; —··—, $\frac{3}{2}\Gamma_R(\partial r_c^2/\partial t)\,(\partial \sin(2\phi)/\partial t)$.

The comparison between equation (13) and the source strength of the weaker vortex (Figure 21) shows the importance of vorticity centroid dynamics in the overall sound production by the weaker vortex, especially within the first cycle even when the vortex core is severely deformed. The slight deviation at $\omega t > 140$ is again nearly sinusoidal (Figure 21). The situation here is similar to that observed during identical vortex coalescence where the peaks and troughs of the pressure fluctuations are related to the rate of "folding up" of core fluids (Figure 15). The peaks and troughs in the slight deviation at $\omega t > 140$ observed in Figure 21 are related to the rate of the weaker vortex "wrapping round" the stronger vortex core. The present insignificance of the core deformation in the sound generation process is not surprising, as one can deduce from equation (15) that the thin strip of vorticity leads to a vanishing S''.

Though the stronger and weaker vortices generate sound through different mechanisms, the results shown in Figure 20 illustrate that the stronger vortex plays the key role in the overall sound generation.

3.2.3. *Tearing*

At a smaller circulation ratio, some of the fluids from the weaker vortex are torn and induced towards the stronger vortex, forming a thin strip of vorticity. The remaining weaker vortex fluids remain intact so that a finite weaker vortex core still exists. This interaction is referred to as "tearing" in the present study. A typical example of such interaction is shown in Figure 22 ($\Gamma_L/\Gamma_R = 2$, $\sigma_L/\sigma_R = 1$ and $G/\sigma_L = 4$). The tip of the vorticity strip moves gradually towards the stronger vortex core boundary under the action of the induced velocity field of the stronger vortex.

The source strength of the stronger vortex appears similar to those presented before. Both the high- and low-frequency components are observed (Figure 23(a)). Again, the low-frequency one is due to the vorticity centroid dynamics, while the stronger high-frequency one is due to the core deformation (not shown here). Since the motion of the vorticity centroid of this stronger vortex is weak when the vorticity bearing fluid from the

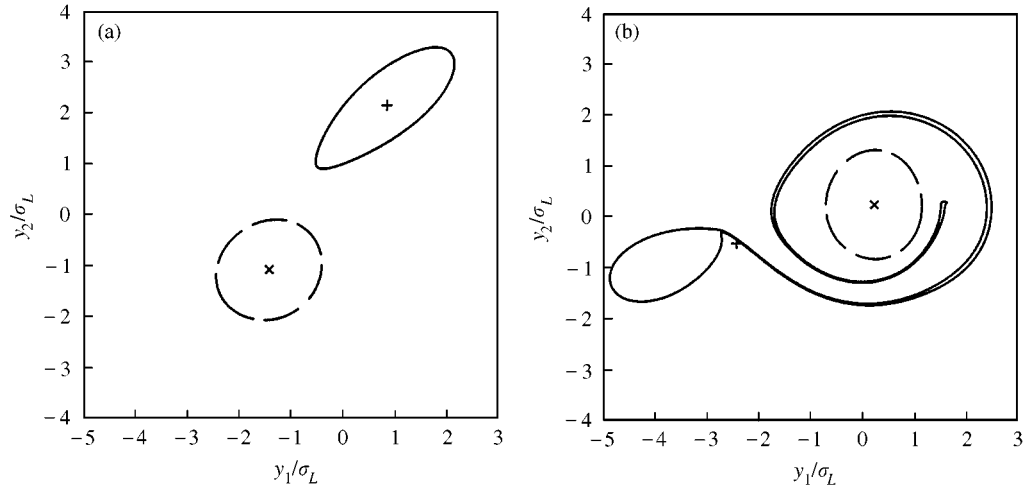

Figure 22. Core evolution under tearing. $\Gamma_L/\Gamma_R = 2$, $G/\sigma_L = 4$, $\sigma_L/\sigma_R = 1$. (a) $\omega t = 20$; (b) $\omega t = 75$. Legends: same as those in Figure 16.

weaker vortex wraps round its core, the final sound production is mainly from its core deformation. The unbalanced vorticity distribution close to the stronger vortex results in a more rigorous core deformation rate and thus the higher sound energy radiation observed in Figure 23(a).

The source strength $\partial^3 S_1/\partial t^3$ of the weaker vortex also contains a high and a relatively lower frequency component, with the latter dominating the sound generation before the vortex core is severely deformed (Figure 23(b)). The high-frequency component is more related to the core deformation mechanism. A similar phenomenon is observed for $\partial^3 S_2/\partial t^3$ and thus not presented. It can also be noted from Figure 23(b) that the vorticity centroid dynamic is the major source of sound for $\omega t < 30$. After that, the two mechanisms (vorticity centroid dynamics and core deformation) counteract with each other in a way similar to that in the case of identical vortex coalescence (Figure 12). The source strength produced by the core deformation becomes dominant for $\omega t > 50$. A strip of vorticity is formed around the stronger vortex by this instant. Together with the observation in Figure 23(a), it can be concluded that the deformations of the two interacting vortex cores are the main sources of sound at increased flight time. Though the contributions from the two vortices are similar at the beginning of the interaction, the stronger vortex is mainly responsible for the sound generation after the weaker vortex is seriously deformed. This is common in the interaction of unequal vortices.

4. CONCLUSIONS

The sound generation mechanisms of inviscid two-dimensional vortex interactions at low Mach number are discussed in detail in the present investigation. The vortex interactions are studied by using the method of contour dynamics, while the sound so generated is studied by using basically the vortex sound theory. Two distinctive sound mechanisms, due to the vorticity centroid dynamics and the unsteady core deformation (microscopic core dynamics), are derived explicitly from the vortex sound theory and confirmed by the numerical results obtained.

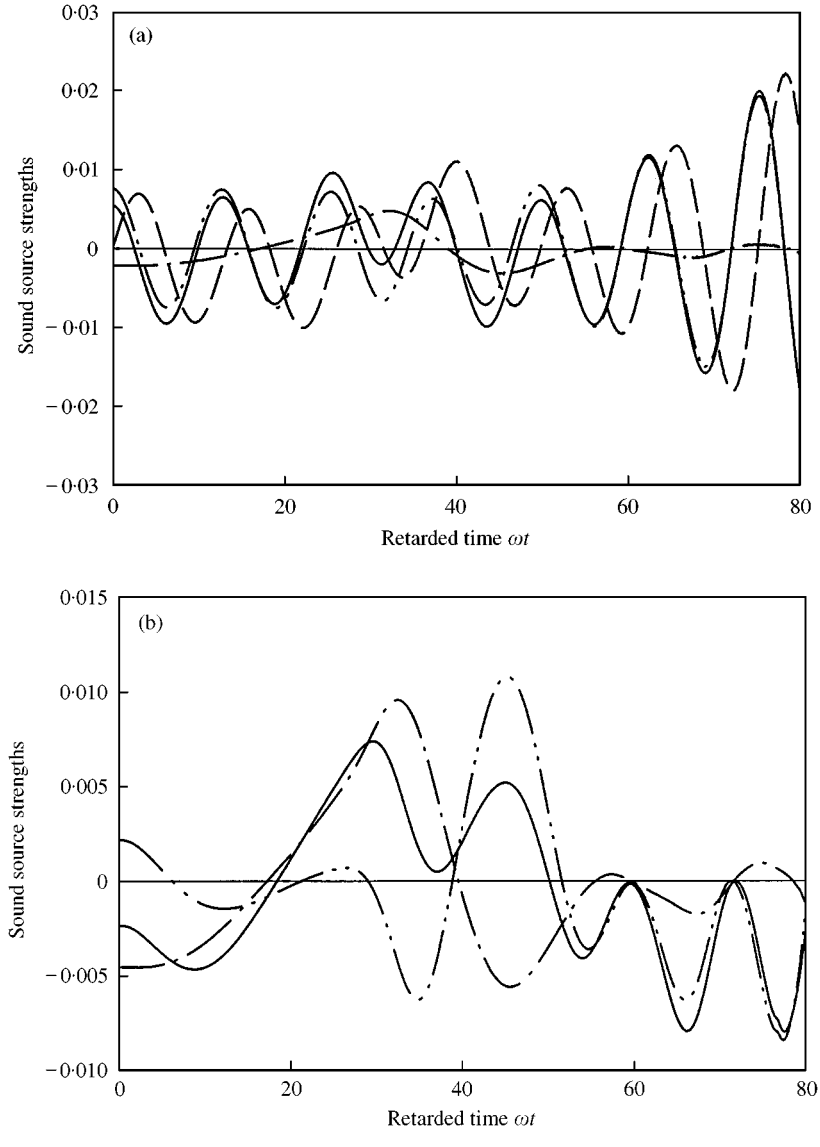

Figure 23. Time variations of source strengths of both vortices under tearing. $\Gamma_L/\Gamma_R = 2$, $G/\sigma_L = 4$, $\sigma_L/\sigma_R = 1$. (a) Stronger vortex; (b) weaker vortex: ——, $\partial^3 S_1/\partial t^3$; — —, $\partial^3 S_2/\partial t^3$; —·—, $\partial^3 S_{polar}/\partial t^3$; —··—, $\partial^3 S''/\partial t^3$.

For identical vortices, only two types of interactions are observed. They are the leapfrogging and coalescence. For the leapfrogging, the sound produced by vorticity centroid dynamics is of low frequency, while that generated by the core deformation is of higher frequency. The amplitude of the former is proportional to the third power of the centroid angular speed, which is essentially a time invariant. It is shown explicitly, through the use of an elliptical core assumption, that the amplitude of the sound generated by the core deformation depends on the rate of change of the differential radius and the rotational speed of the core principle axes. The sounds generated by these mechanisms do not appear to be related to each other.

For the coalescence case, these two mechanisms counteract with each other, resulting in a low-frequency sound radiation that does not depend on the vorticity centroid dynamics. The time variation of these source strength fluctuations correlate well with that of the vorticity centroid location. It is found that the amplitude of the sound is related to the rate of folding up of the vortex cores. Its frequency equals that of the core folding up.

For unequal vortices, three types of interactions are observed. The first one is the leapfrogging and the findings are the same as those in the identical vortex leapfrogging case, except that the low-frequency sound from the weaker vortex is stronger, while the opposite is found for the high-frequency one. The second type of interaction is observed when one of the vortices is substantially stronger than the other so that the weaker vortex core is sheared into a thin vorticity strip. The stronger vortex dominates the overall sound energy radiation. The major sound generation mechanism is the rate of core deformation of the stronger vortex. The weaker vortex produces sound basically through its vorticity centroid dynamics, but is insignificant in the overall sound generation. The third type is the "tearing", where part of the weaker vortex core fluid is torn and forms a strip of vorticity around the stronger vortex core. Again, the sound from the stronger vortex contains both the high- and low-frequency components, which are produced through the two mechanisms discussed above. The core deformation becomes the major source of sound after the vorticity strip from the weaker vortex wraps round the stronger vortex core. The sound produced by the weaker vortex in the beginning of the interaction shows the characteristics of those in the identical vortex coalescence case. The contribution from the vorticity centroid dynamics becomes insignificant at increased time of interaction.

The present theoretical deductions are not limited to a particular vortex core shape, though the vortices are initially assumed to have circular cores. The present results are, therefore, general for sound generation by all inviscid two-dimensional vortex interactions at low Mach number.

ACKNOWLEDGMENTS

This study was partially supported by a research grant from the Committee of Conference and Research Grants, The University of Hong Kong and by a donation from Dr Haking Wong.

REFERENCES

1. M. J. LIGHTHILL 1952 *Proceedings of the Royal Society of London, Series A* **221**, 564–587. On sound generated aerodynamically. I. General theory.
2. S. C. CROW 1970 *Studies of Applied Mathematics* **49**, 21–44. Aerodynamic sound emission as a singular perturbation problem.
3. A. POWELL 1964 *Journal of the Acoustical Society of America* **36**, 177–195. Vortex sound theory.
4. J. E. FFOWCS WILLIAMS and A. J. KEMPTON 1978 *Journal of Fluid Mechanics* **84**, 673–694. The noise from the large-scale structure of a jet.
5. P. DOAK 1998 *Theoretical and Computational Fluid Dynamics* **10**, 115–133. Fluctuating total enthalpy as the basic generalized acoustic field.
6. T. COLONIUS, S. K. LELE and P. MOIN 1997 *Journal of Fluid Mechanics* **330**, 375–409. Sound generation in a mixing layer.
7. B. E. MITCHELL, S. K. LELE and P. MOIN 1999 *Journal of Fluid Mechanics* **383**, 113–142. Direct computation of the sound generated by vortex pairing in an axisymmetric jet.
8. E. ACTON 1972 *Journal of Fluid Mechanics* **76**, 561–592. The modelling of large eddies in a two-dimensional shear layer.

9. P. K. STANSBY and A. SLAOUTI 1993 *International Journal of Numerical Methods on Fluids* **17**, 1003–1013. Simulation of vortex shedding including blockage by the random-vortex and other methods.
10. W. MÖHRING 1978 *Journal of Fluid Mechanics* **85**, 685–691. On the vortex sound at low Mach number.
11. R. C. K LEUNG, S. K. TANG , I. C. K. HO and N. W. M. KO 1996 *American Institute of Aeronautics and Astronautics Journal* **34**, 669–675. Vortex pairing as a model for jet noise generation.
12. S. K. TANG and N. W. M. KO 1995 *Journal of Sound and Vibration* **187**, 287–310. On the sound generated from the interaction of two inviscid coaxial vortex rings moving in the same direction.
13. S. K. TANG and N. W. M. KO 1995 *Journal of the Acoustical Society of America* **98**, 3418–3427. Sound generation by a vortex ring collision.
14. S. K. TANG and N. W. M. KO 1997 *Journal of the Acoustical Society of America* **102**, 1463–1473. Sound generation by interaction of two inviscid two-dimensional vortices.
15. J. LAUFER and T. YEN 1983 *Journal of Fluid Mechanics* **134**, 1–31. Noise generation by a low-Mach-number jet.
16. S. K. TANG and N. W. M. KO 1993 *Transactions of the American Society of Engineers*: *Journal of Fluids Engineering* **115**, 425–435. A study on the noise generation mechanism in a circular jet.
17. C. D. WINANT and F. K. BROWAND 1974 *Journal of Fluid Mechanics* **63**, 237–255. Vortex pairing: the mechanism of turbulent mixing layer growth at moderate Reynolds number.
18. N. J. ZABUSKY, M. H. HUGHES and K. V. ROBERTS 1979 *Journal of Computational Physics* **30**, 96–106. Contour dynamics for the Euler equations in two dimensions.
19. D. G. DRITSCHEL 1986 *Journal of Fluid Mechanics* **172**, 157–182. The nonlinear evolution of rotating configurations of uniform vorticity.
20. W. MÖHRING 1979 in *Mechanism of Sound Generation in Flows* (E.-A. Müller, editor), 85–96. Berlin: Springer. Modelling low Mach number noise.
21. B. E. MITCHELL, S. K. LELE and P. MOIN 1995 *Journal of Fluid Mechanics* **285**, 181–202. Direct computation of the sound from a compressible co-rotating vortex pair.
22. J. E. FFOWCS WILLIAMS and D. L. HAWKINGS 1968 *Journal of Fluid Mechanics* **31**, 779–788. Shallow water wave generation by unsteady flow.
23. K. SHARIFF, A. LEONARD, N. J. ZABUSKY and J. H. FERZIGER 1988 *Fluid Dynamics Research* **3**, 337–343. Acoustics and dynamics of coaxial interacting vortex rings.
24. P. A. JACOBS and D. I. PULLIN 1985 *Physics of Fluids* **28**, 1619–1625. Coalescence of stretching vortices.